POLITECNICO DI TORINO
Repository ISTITUZIONALE

A new boundary element integration strategy for retarded potential boundary integral equations

Original
A new boundary element integration strategy for retarded potential boundary integral equations / Falletta, Silvia; Scuderi, Letizia. - In: APPLIED NUMERICAL MATHEMATICS. - ISSN 0168-9274. - 94:(2015), pp. 106-126. [10.1016/j.apnum.2015.03.009]

Availability:
This version is available at: 11583/2535122 since: 2019-09-04T15:32:14Z

Publisher:
Elsevier

Published
DOI:10.1016/j.apnum.2015.03.009

Terms of use:
openAccess

This article is made available under terms and conditions as specified in the corresponding bibliographic description in the repository

Publisher copyright

(Article begins on next page)

05 May 2023

A new boundary element integration strategy for retarded potential boundary integral equations *

S. Falletta†, L. Scuderi‡

Abstract

We consider the retarded potential boundary integral equation, arising from the 3D Dirichlet exterior wave equation problem. For its numerical solution we use compactly supported temporal basis functions in time and a standard collocation method in space. Since the accurate computation of the integrals involved in the numerical scheme is a key issue for the numerical stability, we propose a new efficient and competitive quadrature strategy. We compare this approach with the one that uses the Lubich time convolution quadrature, and show pros and cons of both methods.

Key words: 3D wave equation; time dependent boundary integral equations; quadrature formulas.

1 Introduction

Let $\Omega^i \subset \mathbb{R}^3$ be an open bounded domain with a sufficiently smooth boundary Γ. We define $\Omega := \mathbb{R}^3 \setminus \bar{\Omega}^i$ and we consider the following exterior homogeneous wave equation with a Dirichlet boundary condition on the surface Γ and homogeneous initial conditions:

$$\begin{cases} \Delta u(\mathbf{x},t) - u_{tt}(\mathbf{x},t) = 0 & \text{in } \Omega \times (0,T), \\ u(\mathbf{x},t) = g(\mathbf{x},t) & \text{in } \Gamma \times (0,T), \\ u(\mathbf{x},0) = 0 & \text{in } \Omega, \\ u_t(\mathbf{x},0) = 0 & \text{in } \Omega. \end{cases} \tag{1}$$

It is well known that the following single-layer potential representation of u

$$u(\mathbf{x},t) = \int_\Gamma \int_0^t G(||\mathbf{x}-\mathbf{y}||, t-\tau)\varphi(\mathbf{y},\tau)\, d\tau\, d\Gamma_{\mathbf{y}} \quad \mathbf{x} \in \Omega, \quad t \in [0,T] \tag{2}$$

*This work was supported by the Ministero dell'Istruzione, dell'Università e della Ricerca of Italy, under the research program PRIN09: Boundary element methods for time dependent problems, and by the GNCS-INDAM 2013 research program: Metodi fast per la risoluzione numerica di sistemi di equazioni integro-differenziali.

†Dipartimento di Scienze Matematiche, Politecnico di Torino, Italy. Email: silvia.falletta@polito.it

‡Dipartimento di Scienze Matematiche, Politecnico di Torino, Italy. Email: letizia.scuderi@polito.it

holds, where $G(\mathbf{x},t)$ denotes the fundamental solution

$$G(r,t)=\frac{1}{4\pi}\frac{\delta(t-r)}{r},\qquad r=||\mathbf{x}-\mathbf{y}||, \tag{3}$$

being $\delta(\cdot)$ the Dirac delta function. The function φ in (2) is the solution of the following Time Dependent Boundary Integral Equation (TDBIE)

$$\int_\Gamma\int_0^t G(r,t-\tau)\varphi(\mathbf{y},\tau)\,d\tau d\Gamma_{\mathbf{y}}=g(\mathbf{x},t),\quad \mathbf{x}\in\Gamma,\quad t\in[0,T] \tag{4}$$

and represents the jump of the normal derivative of u along Γ.

We assume here that the boundary Γ of the domain Ω and the boundary data satisfy the regularity and compatibility properties which guarantee existence and uniqueness of a classical solution of the problem in $C^2([0,T],C^2(\bar{\Omega}))$. For a result on existence and uniqueness of the solution of (4) in a proper function space setting, see [4].

Several numerical approaches have been proposed for solving wave equation problems by means of BIEs. Among all, we mention the pioneering work by Bamberger and Ha Duong for the scattering problems in the frequency domain [4], the Lubich convolution quadrature method [11] and the more recent energetic approach [2, 3] for solving time dependent boundary integral equations. In [4, 11], theoretical results on stability and convergence are also proved. In all the mentioned papers, a Galerkin approximation scheme in space is considered, and the stability result holds admitted that the matrix elements, defined by space integrals, are computed analytically. In practice, such elements are approximated with a certain accuracy ε; such an approximation may cause instability phenomena that depend on the choice of the time and space discretization parameters.

In [11], Lemma 5.5, Lubich proved that, for a fixed T, if all the matrix elements are computed with a tolerance ε, then there exists a time step $\Delta_{t,0}$ depending on ε (equivalently, a maximum number of time steps $N_0=N_0(\varepsilon)$), such that the method is unstable for all the values of $\Delta_t<\Delta_{t,0}$ (equivalently, for all $N>N_0$). Therefore, time steps too small are not allowed, unless the integrals are computed with a sufficiently high accuracy. This phenomenon has been observed also in [15].

As an alternative approach to the Galerkin method, one may consider to couple the Lubich technique with a collocation scheme, which is cheaper than the Galerkin method, because it requires the computation of only single space integrals. However, drawbacks similar to those mentioned above occur, when a space collocation method is applied. Even if so far there are no theoretical results about stability and convergence, based on the performed numerical tests, we conjecture that all the above considerations concerning the stability on the Galerkin scheme hold for the collocation method as well.

By taking into account the presence of the Dirac delta function in the expression of the fundamental solution (3), and performing the analytical integration with respect to the τ variable, equation (4) becomes

$$\frac{1}{4\pi}\int_\Gamma\frac{\varphi(\mathbf{y},t-r)}{r}d\Gamma_{\mathbf{y}}=g(\mathbf{x},t),\quad \mathbf{x}\in\Gamma,\quad t\in[0,T]. \tag{5}$$

The latter is referred as retarded potential boundary integral equation.

Very recently ([5, 14]), a new time approach has been proposed for the solution of (5). This consists in performing an approximation in time by taking a linear combination of compactly supported temporal basis functions. Such an approach has been proposed in [5] for the discretization of some Volterra integral equations and then combined with Galerkin and collocation space schemes for the solution of the retarded BIE (5). In [14] the authors propose a similar technique for a space time Galerkin approximation to solve (5) with an adaptive strategy in time.

The advantages of this time approach, with respect to the Lubich one, are the analytic integration in time and the locality of the support of the temporal basis functions. This latter property implies that many elements of the final linear system are null. Moreover, it is possible to detect a priori which matrix elements have to be computed and stored. Therefore the final linear system has a sparse structure, which allows to reduce the computational cost and the memory storage. The same property does not hold for the Lubich approach, because the coefficients involved in the convolution quadrature technique have a global support; hence all the system elements must be computed and stored. However, we recall here that they are computed simultaneously by using the FFT, with a low computational cost. Moreover, we mention that, because of the behavior of the convolution coefficients, the system element matrices of the final linear system could be approximated by corresponding sparse ones by using a suitable strategy (see [9]), since they represent a smooth approximation of the delta Dirac function ([12]). Unfortunately, this strategy does not allow the use of the FFT. Therefore, to take advantage of the FFT benefits, one has to compute and store all of them first, and cut the negligible elements only afterwards.

However, as for the Lubich technique, we have noticed the importance of the accurate computation of the matrix elements for the method based on compactly supported temporal basis functions as well, both in the Galerkin and in the collocation space approach. In particular, the numerical tests we have performed highlight that, for a given final time T, the higher is the accuracy of the system elements, the smaller is the time step Δ_t we can choose. Moreover, since another key issue is the possibility of choosing long times T, we are interested in fixing Δ_t and increasing the number of time steps N. We have noticed that, if the all the matrix elements are computed with a tolerance ε, there exists a maximum number of time steps $N_0 = N_0(\varepsilon)$ such that the method is unstable for all $N > N_0$. In this case too, the higher is the accuracy of the system elements, the longer is the interval of integration $[0, T_0]$, $T_0 = N_0\Delta_t$, where no instability phenomena show up. Thus, the efficient and accurate computation of all the integrals which define the linear system is a key issue for the success of the corresponding method, whatever it is. Incidentally, we point out that similar considerations hold true for the energetic formulation in [1], and for the Lubich collocation method applied in [8] to solve a 2D Neumann problem; in both papers the authors use ad hoc quadrature formulas.

In this paper we analyze and test the above mentioned numerical approaches for the solution of the BIEs (4) and (5), based on the Lubich technique and on the use of compactly supported temporal basis functions for the time approximation, respectively; these are then combined with a collocation scheme for the space discretization. In particular, we focus on

the computation of the matrix system elements, which are given by space integrals. If a standard quadrature formula is applied to approximate such integrals, in order to improve the accuracy of the approximation it would be sufficient, in principle, to increase the number of the quadrature nodes. This procedure can be successfully applied in the Lubich approach; unfortunately, in the case of compactly supported basis functions in time, it requires a very large number of quadrature nodes when the integrand function (which has a compact support) is significant only in a very small region. For this reason, we propose a new strategy based on the exact detection of the support of the integrand function, that allows to compute efficiently the above integrals by using few quadrature nodes. As the numerical tests show, this strategy significantly increases the efficiency of the numerical method based on compactly supported temporal basis functions, coupled with a collocation scheme in space. However, on the ground of the numerical tests performed, this method seems to be conditionally stable; indeed, for a fixed space mesh, even if the matrix elements are computed with a very high accuracy, numerical instabilities show up unless the time step is chosen sufficiently small. Since this phenomenon does not occur in the Lubich collocation method, we conjecture that the latter is stable and, therefore, more reliable and robust for numerical applications.

Incidentally, we remark that if a non homogeneous equation and/or non vanishing initial data and initial velocity are considered, the same approaches can be applied as well. In fact, in that case three "volume" integral terms have to be added to the known term of the BIEs (4) and (5). Since for their numerical computation some efficient formulas have been already proposed in [7], here we will only consider the full homogeneous problem.

2 Spatial and temporal approximations

For the space discretization, the surface Γ is approximated by that of a polyhedron Γ_Δ having triangular faces; we denote by Δ_x the mesh size, which is given by the maximum triangle diameter. For any fixed $t \in [0, T]$, the unknown function φ is approximated by

$$\varphi(\mathbf{x}, t) \approx \varphi_{\Delta_x}(\mathbf{x}, t) := \sum_{i=1}^{M} \varphi_i(t) b_i(\mathbf{x}) \tag{6}$$

where $\varphi_i(t) \approx \varphi(\mathbf{x}_i, t)$, being $\mathbf{x}_i$ the vertices of the triangular decomposition of the surface; $\{b_i\}_{i=1}^M$ denotes the set of the piecewise linear basis functions defined on a regular boundary element mesh on Γ_Δ, and M is the total number of vertices of the chosen triangulation.

For the time approximation, we choose a uniform partition of the interval $[0, T]$ into N subintervals of equal length $\Delta_t = T/N$. Then we consider two approaches: the first one is based on the Lubich convolution quadrature rule applied to (4) (see [10, 7]); the second one on the approximation by means of compactly supported temporal basis functions applied to (5) (see [5, 14]).

In Sections 2.1 and 2.2 we recall the main ideas of both strategies combined with a standard collocation method in space. In Section 3 we detail the quadrature formulas that are used to compute the space integrals involved in the resolution of the BIEs (4) and (5) for both approaches. In particular, we propose a new strategy for the numerical computation of

the integrals when compactly supported basis functions in time are used. Such a strategy is based on the exact detection of the support of the integrand functions and allows to compute efficiently the involved space integrals with few quadrature nodes.

2.1 Lubich convolution quadrature in time and collocation in space

As a first approach, we discretize the time integral in (4) by means of the Lubich convolution quadrature rule, and we use a standard collocation method for the space discretization. We will refer to it by using the label $\mathcal{L}$. This approach has been already considered in [7]. In the following we recall the main ingredients of this strategy.

We first approximate the unknown solution by (6), and we collocate the equation at the discrete time levels $t_n = n\Delta_t$, $n = 0, \ldots, N$. The semidiscretization of (4) takes the form

$$\sum_{i=1}^{M} \int_{\mathcal{S}_i} \left(\int_0^{t_n} G(r, t_n - \tau)\varphi_i(\tau)\, d\tau \right) b_i(\mathbf{y})\, d\Gamma_{\mathbf{y}} = g(\mathbf{x}, t_n), \quad \mathbf{x} \in \Gamma_\Delta,\ n = 0, \ldots, N;$$

$\mathcal{S}_i = \cup_{\ell=1}^{n_i} \mathcal{T}_\ell$ denotes the union of the triangles having the common vertex in $\mathbf{x}_i$, where the shape function b_i is non vanishing and satisfies $b_i(\mathbf{x}_i) = 1$. Then we discretize the time integrals by means of the Lubich convolution quadrature rule associated with the Backward Difference Formula (BDF) of order 2 for ODE initial value problems (see [10]). We obtain

$$\sum_{j=0}^{n} \sum_{i=1}^{M} \varphi_i^j \int_{\mathcal{S}_i} \omega_{n-j}(\Delta_t; r) b_i(\mathbf{y})\, d\Gamma_{\mathbf{y}} = g(\mathbf{x}, t_n), \quad \mathbf{x} \in \Gamma_\Delta, \quad n = 0, \ldots, N, \tag{7}$$

where $\varphi_i^j \approx \varphi(\mathbf{y}_i, t_j)$. The coefficients ω_n in (7) are defined by

$$\omega_n(\Delta_t; r) = \frac{1}{2\pi i} \int_{|z|=\rho} K\left(r, \frac{\gamma(z)}{\Delta_t}\right) z^{-(n+1)}\, dz, \tag{8}$$

where

$$K(r, z) = \frac{e^{-rz}}{4\pi\, r} \tag{9}$$

is the Laplace transform of the fundamental solution G, $\gamma(z) = 3/2 - 2z + 1/2z^2$ is the characteristic quotient of the BDF method of order 2, and ρ is such that for $|z| \le \rho$ the corresponding $\gamma(z)$ lies in the domain of analyticity of K. By introducing the polar coordinate $z = \rho e^{\imath\theta}$, the integrals in (8) can be efficiently computed by a trapezoidal rule with L equal steps of length $2\pi/L$:

$$\omega_n(\Delta_t; r) \approx \frac{\rho^{-n}}{L} \sum_{l=0}^{L-1} K\left(r, \frac{\gamma(\rho e^{\frac{\imath l 2\pi}{L}})}{\Delta_t}\right) e^{-\frac{\imath n l 2\pi}{L}}. \tag{10}$$

In [10], Lubich has suggested to choose $L = 2N$ and $\rho^N = \sqrt{\varepsilon}$ since these choices lead to an approximation of ω_n with relative error of size $\sqrt{\varepsilon}$, if K is computed with a relative accuracy bounded by ε. We choose here $\varepsilon = 10^{-14}$ so that, according to the previous statement,

this should give a relative accuracy of order 10^{-7}, which is sufficient for the tests we have performed and that we will present in Section 4. All the ω_n are computed simultaneously by the FFT, with $O(N \log N)$ flops.

By applying the standard collocation method, the final discrete problem consists of finding the coefficients φ_i^n of the approximating function

$$\varphi_{\Delta_t,\Delta_x}(\mathbf{y}, t_n) = \sum_{i=1}^{M} \varphi_i^n b_i(\mathbf{y}), \qquad n = 0, \ldots, N$$

such that

$$\sum_{j=0}^{n} \sum_{i=1}^{M} \varphi_i^j \int_{\mathcal{S}_i} \omega_{n-j}(\Delta_t; r_m) b_i(\mathbf{y})\, d\Gamma_{\mathbf{y}} = g(\mathbf{x}_m, t_n), \quad n = 0, \ldots, N \tag{11}$$

where $r_m = \|\mathbf{x}_m - \mathbf{y}\|$, being $\mathbf{x}_m$, $m = 1, \ldots, M$, the collocation points coinciding with the vertices of the mesh triangles. Finally, replacing (9) and (10) in (11), we get

$$\frac{1}{4\pi} \sum_{j=0}^{n} \frac{\rho^{-(n-j)}}{L} \sum_{i=1}^{M} \varphi_i^j \sum_{l=0}^{L-1} \left(\int_{\mathcal{S}_i} \frac{e^{-r_m \zeta_l}}{r_m} b_i(\mathbf{y})\, d\Gamma_{\mathbf{y}} \right) e^{-\frac{\imath(n-j)l2\pi}{L}} = g(\mathbf{x}_m, t_n), \tag{12}$$

$m = 1, \ldots, M,\ n = 0, \ldots, N$, where $\zeta_l = \gamma(\rho e^{\frac{\imath l 2\pi}{L}})/\Delta_t$. The Lubich-collocation method leads to a Toeplitz block lower triangular linear system of the form

$$\sum_{j=0}^{n} \mathbf{A}_{n-j} \boldsymbol{\varphi}^j = \mathbf{g}_n, \qquad n = 0, \ldots, N, \tag{13}$$

in the unknown vectors $\boldsymbol{\varphi}^j = (\varphi_1^j, \ldots, \varphi_M^j)^T$, $j = 0, \ldots, N$. Since $\mathbf{A}_0$ turns out to be nonsingular and $g(\mathbf{x}, t_0) \equiv u(\mathbf{x}, t_0) = 0$ (for the compatibility conditions on the data), we have $\boldsymbol{\varphi}^0 = \mathbf{0}$.

2.2 Compactly supported basis functions in time and collocation in space

Following [5] and [14], an approach for the discretization of (5) in time is obtained by using temporal compactly supported basis functions. In the sequel, we will refer to it by using the label $\mathcal{CB}$.

We first approximate the unknown solution by (6) and we collocate the resulting equation at $t = t_n$. The semidiscretization of (5) takes the form

$$\frac{1}{4\pi} \sum_{i=1}^{M} \int_{\mathcal{S}_i} \frac{\varphi_i(t_n - r) b_i(\mathbf{y})}{r} d\Gamma_{\mathbf{y}} = g(\mathbf{x}, t_n), \quad n = 0, \ldots, N.$$

Finally, we approximate each coefficient $\varphi_i(t_n - r)$ by a linear combination of suitable basis functions $\{N_j\}_{j=0}^{N}$, compactly supported and satisfying the property $N_j(t_n - r) = N_{n-j}(r)$. We obtain:

$$\varphi_i(t_n - r) \approx \sum_{j=0}^{n} \bar{\varphi}_i^j N_j(t_n - r) = \sum_{j=0}^{n} \bar{\varphi}_i^{n-j} N_j(r),$$

where $\bar{\varphi}_i^j \approx \varphi(\mathbf{y}_i, t_j)$. Since the explicit choice of the N_j's is not a key issue here, they will be specified in the section devoted to the numerical experiments.

By applying the space collocation method, the final discrete problem consists of finding the coefficients $\bar{\varphi}_i^n$ of the approximating function

$$\bar{\varphi}_{\Delta_x,\Delta_t}(\mathbf{y}, t_n - r) = \sum_{i=1}^{M} \sum_{j=0}^{n} \bar{\varphi}_i^{n-j} N_j(r) b_i(\mathbf{y})$$

such that

$$\frac{1}{4\pi} \sum_{j=0}^{n} \sum_{i=1}^{M} \bar{\varphi}_i^{n-j} \int_{\mathcal{S}_i} \frac{N_j(r_m) b_i(\mathbf{y})}{r_m} d\Gamma_{\mathbf{y}} = g(\mathbf{x}_m, t_n), \quad n = 0, \ldots, N \tag{14}$$

holds for $\mathbf{x} \equiv \mathbf{x}_m$, $m = 1, \ldots, M$. As in the Lubich approach, the final linear system has a Toeplitz block lower triangular structure, as follows

$$\sum_{j=0}^{n} \bar{\mathbf{A}}_j \bar{\boldsymbol{\varphi}}^{n-j} = \mathbf{g}_n, \qquad n = 0, \ldots, N, \tag{15}$$

in the unknown vectors $\bar{\boldsymbol{\varphi}}^j = (\bar{\varphi}_1^j, \ldots, \bar{\varphi}_M^j)^T$, $j = 0, \ldots, N$.

Remark 2.1 *Due to the locality of the support of the temporal basis functions N_j, all the blocks $\bar{\mathbf{A}}_j$ are sparse and the final Toeplitz matrix is not only lower triangular, but can also have a lower band structure. In fact, denoting by D the diameter of the boundary Γ, it is not difficult to prove that all the matrices $\bar{\mathbf{A}}_j$ are null for all $j \geq J$, where $J = \min\{N, \lfloor \frac{D}{T} N \rfloor\}$. Therefore, for $T > D$, the lower band width is smaller than N and it decreases as T increases. The sparsity structure allows to reduce the computational cost and the memory storage (see Section 4, Tables 4 and 5 for the numerical details). The sparsity property does not hold for the Lubich approach, where all the $N+1$ matrices $\mathbf{A}_j$ must be computed and stored, and are full. However we mention here that, because of the behavior of the coefficients ω_n in the Lubich convolution quadrature formula, the matrices $\mathbf{A}_j$ could be approximated by corresponding very sparse ones (see [9]), since the coefficients represent a smooth approximation of the delta Dirac function (see [12]).*

3 Quadrature formulas for the space integrals

In this section we focus on the efficient computation of the space integrals appearing in (12) and in (14), which is essential for the numerical stability of the corresponding method. Taking into account the linearity of the integral, we can reduce the integral over $\mathcal{S}_i$ to the sum of the integrals over the triangles $\mathcal{T}_\ell$, $\ell = 1, \cdots, n_i$. Therefore, we consider the following benchmark integrals:

$$I_{\mathcal{L}} := \int_{\mathcal{T}} \frac{e^{-r_m \zeta}}{r_m} b_i(\mathbf{y})\, d\mathbf{y}, \tag{16}$$

for the approach $\mathcal{L}$, and

$$I_{\mathcal{CB}} := \int_{\mathcal{T}} \frac{N_j(r_m) b_i(\mathbf{y})}{r_m}\, d\mathbf{y}, \tag{17}$$

for the approach $\mathcal{CB}$, with $r_m = \|\mathbf{x}_m - \mathbf{y}\|$, $\mathcal{T} = \mathcal{T}_\ell$ for a certain ℓ and $\zeta = \zeta_l$. In particular, we propose a new strategy to compute the integrals (17) accurately and with few quadrature nodes.

We denote by $\mathbf{P}_j = (P_{1,j}, P_{2,j}, P_{3,j})$, $j = 1, 2, 3$ the vertices of the triangle $\mathcal{T}$ and, without loss of generality, we choose $\mathbf{P}_1$ such that $\mathbf{P}_1 \equiv \mathbf{x}_i$, in order to guarantee that $b_i(\mathbf{P}_1) = 1$. Denoting by $\widehat{\mathcal{T}}$ the reference triangle of vertices $(0,0), (1,0), (0,1)$, let $\mathbf{y} = M_{\mathcal{T}}(\hat{\mathbf{y}})$, with $\hat{\mathbf{y}} = (\hat{y}_1, \hat{y}_2) \in \widehat{\mathcal{T}}$, be the parametrization of the triangle $\mathcal{T}$, defined as follows:

$$\mathbf{y} = P_1 + (P_2 - P_1)\hat{y}_1 + (P_3 - P_1)\hat{y}_2, \quad 0 \le \hat{y}_1 \le 1, 0 \le \hat{y}_2 \le 1 - \hat{y}_1.$$

According to the above choices, we easily find that $\hat{b}_i(\hat{\mathbf{y}}) := b_i(M_{\mathcal{T}}(\hat{\mathbf{y}}))$ is the fundamental basis function $\hat{b}_i(\hat{y}_1, \hat{y}_2) := 1 - \hat{y}_1 - \hat{y}_2$ defined on the reference triangle $\widehat{\mathcal{T}}$. Introducing the above parametrization, the integrals $I_{\mathcal{L}}$ and $I_{\mathcal{CB}}$ become

$$I_{\mathcal{L}} = 2Area(\mathcal{T}) \int_{\widehat{\mathcal{T}}} \frac{e^{-r_m\zeta}}{r_m} \hat{b}_i(\hat{\mathbf{y}})\, d\hat{\mathbf{y}}, \tag{18}$$

and

$$I_{\mathcal{CB}} = 2Area(\mathcal{T}) \int_{\widehat{\mathcal{T}}} \frac{N_j(r_m)\hat{b}_i(\hat{\mathbf{y}})}{r_m} d\hat{\mathbf{y}}, \tag{19}$$

with $r_m = \|\mathbf{x}_m - M_{\mathcal{T}}(\hat{y})\|$. For the numerical computation of $I_{\mathcal{L}}$, we first introduce the polar coordinate $\hat{\mathbf{y}} = \varrho e^{\imath\theta}$, so that

$$I_{\mathcal{L}} = 2Area(\mathcal{T}) \int_0^{\frac{\pi}{2}} \int_0^{\frac{1}{sin\theta + cos\theta}} \frac{e^{-r_m\zeta}}{r_m} \hat{b}_i(\varrho e^{\imath\theta})\varrho\, d\varrho\, d\theta, \qquad r_m = \|\mathbf{x}_m - M_{\mathcal{T}}(\varrho e^{\imath\theta})\|, \tag{20}$$

and we apply the n-point Gauss-Legendre quadrature rule to each integral in (20). The same strategy can in principle be used for the numerical computation of $I_{\mathcal{CB}}$. However, it is worth noting that, in this case, the support of the integrand function is defined by the intersection of the triangle $\widehat{\mathcal{T}}$ with the support of the temporal basis functions N_j. Therefore, since the width of the support of N_j depends on Δ_t and, in particular, it decreases as the time mesh is refined, the support of the integrand function in (19) can be a very small region with respect to $\mathcal{T}$ and when Δ_t is small (see, for example, Figure 5, left plots). In such a case, the integration over the whole triangle is very inefficient, since only few quadrature nodes (that are distributed in the whole $\widehat{\mathcal{T}}$) belong to the support of the integrand function. Since, as we already remarked, numerical instabilities appear in the corresponding numerical method when the integrals are not accurately evaluated, the integration over the whole triangle would require a very large number of nodes (see Tables 2, 3, 6, 7 and Figure 6 in Section 4). For this reason, we have developed a strategy to determine the support of the integrand function and to compute the integral $I_{\mathcal{CB}_{loc}}$ defined as

$$I_{\mathcal{CB}_{loc}} := 2Area(\mathcal{T}) \int_{\widehat{\mathcal{T}} \cap supp(N_j)} \frac{N_j(r_m)\hat{b}_i(\hat{\mathbf{y}})}{r_m} d\hat{\mathbf{y}}. \tag{21}$$

The localization of the domain of integration $\widehat{\mathcal{T}} \cap supp(N_j)$ relies on geometric operations, starting from the following expression of the distance r_m:

$$\begin{aligned} r_m^2 &= \sum_{j=1}^{3}(x_{j,m} - (M_{\mathcal{T}}(\hat{y}))_j)^2 \\ &= \sum_{j=1}^{3}\Big((x_{j,m} - P_{j,1}) - (P_{j,2} - P_{j,1})\hat{y}_1 - (P_{j,3} - P_{j,1})\hat{y}_2\Big)^2 \\ &= a\hat{y}_1^2 + b\hat{y}_2^2 - 2c\hat{y}_1 - 2d\hat{y}_2 + 2e\hat{y}_1\hat{y}_2 + f, \end{aligned} \tag{22}$$

where

$$\begin{aligned} a &= \sum_{j=1}^{3}(P_{j,2} - P_{j,1})^2, & b &= \sum_{j=1}^{3}(P_{j,3} - P_{j,1})^2, \\ c &= \sum_{j=1}^{3}(x_{j,m} - P_{j,1})(P_{j,2} - P_{j,1}), & d &= \sum_{j=1}^{3}(x_{j,m} - P_{j,1})(P_{j,3} - P_{j,1}), \\ e &= \sum_{j=1}^{3}(P_{j,2} - P_{j,1})(P_{j,3} - P_{j,1}), & f &= \sum_{j=1}^{3}(x_{j,m} - P_{j,1})^2. \end{aligned}$$

Equation (22) represents an elliptic paraboloid, with respect to the variables $\hat{y}_1$, $\hat{y}_2$ and r_m^2, whose center (minimum) is $C = (C_1, C_2, r_m^2(C_1, C_2))$, where $C_1 = (cb - ed)/(ab - e^2)$ and $C_2 = (ad - ec)/(ab - e^2)$. In order to obtain the canonical form of the paraboloid, by following a standard procedure, we apply the rototranslation of the axes $\hat{y}_1$ and $\hat{y}_2$, $(\hat{y}_1, \hat{y}_2) = \mathcal{R}(\bar{y}_1, \bar{y}_2)$, defined as follows

$$\begin{cases} \hat{y}_1 = & v_{1,1}\bar{y}_1 + v_{1,2}\bar{y}_2 + C_1 \\ \hat{y}_2 = & v_{2,1}\bar{y}_1 + v_{2,2}\bar{y}_2 + C_2 \end{cases}$$

where $v_1 = (v_{1,1}, v_{2,1})$ and $v_2 = (v_{1,2}, v_{2,2})$ are the orthogonal eigenvectors associated to the positive eigenvalues λ_1 and λ_2 of the symmetric definite positive matrix $\begin{pmatrix} a & e \\ e & b \end{pmatrix}$. We denote by $\bar{\mathcal{T}} = \mathcal{R}^{-1}(\widehat{\mathcal{T}})$, and we remark that the relation $\mathcal{T} = (M_{\mathcal{T}} \circ \mathcal{R})(\bar{\mathcal{T}})$ holds. Hence, the canonical form of (22) becomes

$$r_m^2 = \lambda_1\bar{y}_1^2 + \lambda_1\bar{y}_2^2 + h,$$

with $h = f + aC_1^2 + bC_2^2 - 2cC_1 - 2dC_2 + 2eC_1C_2$.

Now, denoting by $[t_{1,j}, t_{2,j}]$ the support of the generic shape function N_j, and recalling that N_j has to be evaluated in r_m (see (21)), we impose $t_{1,j}^2 \le r_m^2 \le t_{2,j}^2$. Then, we deduce that the function N_j is non vanishing if and only if r_m lies between the two ellipses of equation

$$\begin{aligned} \lambda_1\bar{y}_1^2 + \lambda_2\bar{y}_2^2 &= t_{1,j}^2 - h \\ \lambda_1\bar{y}_1^2 + \lambda_2\bar{y}_2^2 &= t_{2,j}^2 - h, \end{aligned} \tag{23}$$

which are non degenerate for $t_{1,j}^2 > h$ and $t_{2,j}^2 > h$. Denoting by $\varrho_{1,j}^2 = \max\{0, t_{1,j}^2 - h\}$ and $\varrho_{2,j}^2 = \max\{0, t_{2,j}^2 - h\}$, and by $\mathcal{E}(\bar{y}_1, \bar{y}_2) = \lambda_1\bar{y}_1^2 + \lambda_2\bar{y}_2^2$, the integration domain of the transformed integral (21) is the strip

$$\mathcal{C}_j = \{(\bar{y}_1, \bar{y}_2) \in \bar{\mathcal{T}} : \varrho_{1,j}^2 \le \mathcal{E}(\bar{y}_1, \bar{y}_2) \le \varrho_{2,j}^2\}, \tag{24}$$

so that

$$I_{\mathcal{CB}_{loc}} = 2Area(\mathcal{T}) \int_{\mathcal{C}_j} \frac{N_j(r_m)\hat{b}_i(\mathcal{R}(\bar{\mathbf{y}}))}{r_m} d\bar{\mathbf{y}}, \quad r_m = \|\mathbf{x}_m - (M_{\mathcal{T}} \circ \mathcal{R})(\bar{\mathbf{y}})\|. \tag{25}$$

We remark that $\mathcal{C}_j$ may assume different shapes; in particular it may consist of a single or of disjoint regions (see, for example, the plots on the left side of Figure 5). In order to describe the numerical computation of (25), we refer to the case of a single strip as a benchmark configuration, like that represented in Figure 1. To this aim, we introduce in (25) the elliptic coordinates

$$\begin{cases} \bar{y}_1 &= \frac{\varrho}{\sqrt{\lambda_1}} \cos\theta \\ \bar{y}_2 &= \frac{\varrho}{\sqrt{\lambda_2}} \sin\theta, \end{cases}$$

and, to improve further the accuracy of the computation, we split the integration with respect to the variable θ by taking into account all the intersections of the edges of the triangle with the two ellipses. Precisely, we rewrite (25) as follows

$$I_{\mathcal{CB}_{loc}} = \frac{2Area(\mathcal{T})}{\sqrt{\lambda_1\lambda_2}} \sum_{k=1}^{K-1} \int_{\theta_k}^{\theta_{k+1}} \int_{\varrho_{min}}^{\varrho_{max}} \frac{N_j(r_m)\hat{b}_i(\mathcal{R}(\frac{\varrho}{\sqrt{\lambda_1}}\cos\theta, \frac{\varrho}{\sqrt{\lambda_2}}\sin\theta))}{r_m} \varrho d\varrho d\theta, \tag{26}$$

for $r_m = \|\mathbf{x}_m - (M_{\mathcal{T}} \circ \mathcal{R})(\frac{\varrho}{\sqrt{\lambda_1}}\cos\theta, \frac{\varrho}{\sqrt{\lambda_2}}\sin\theta))\|$. The integration is composed of a sequence of integrals over ϱ, along rays at fixed values of θ. The integration limits $\theta_1 \le \theta_2 \le \cdots \le \theta_K$ are the slopes of the rays joining the origin of the axes $\bar{y}_1$, $\bar{y}_2$ with all the intersections of the edges of the triangle with the two ellipses (see Figure 1). For a fixed angle θ, the extremes of integrations $\varrho_{min} = \varrho_{min}(\theta)$ and $\varrho_{max} = \varrho_{max}(\theta)$ are defined as

$$\varrho_{min}(\theta) = \max\{\varrho_{1,j}, \min\{\sigma_1(\theta), \sigma_2(\theta)\}\} \qquad \varrho_{max}(\theta) = \min\{\varrho_{2,j}, \max\{\sigma_1(\theta), \sigma_2(\theta)\}\},$$

where $\sigma_1(\theta)$ and $\sigma_2(\theta)$ are the intersections of the ray having slope θ with the edges of the triangle $\mathcal{T}$ (see Figure 1).

Finally, we apply an n-point Gauss-Legendre quadrature rule both to the interior and exterior integrals. We remark that, in principle, the integration with respect to θ could be carried over the global interval $\theta_{min} := \theta_1$ and $\theta_{max} := \theta_K$; in this case the accuracy of the integral $I_{\mathcal{CB}_{loc}}$ is poor due to the presence of those corners in the integration domain that affect the regularity of the integrand function. Furthermore, when $\mathcal{C}_j$ consists of disjoint strips, $I_{\mathcal{CB}_{loc}}$ is obtained as the sum of integrals of type (26).

We point out that the benefits of these apparently cumbersome calculations are extremely significant. In fact, it is worth noting that the support $[t_{1,j}, t_{2,j}]$ of N_j depends on Δ_t, hence the strip $\mathcal{C}_j$ becomes thinner and thinner as Δ_t decreases or, equivalently, when T is fixed and the number of the time steps N increases. In such a case, the detection of the support of the integrand function plays a key role in the computation of the integral (21); indeed, only few quadrature nodes inside the strip are sufficient to get a good accuracy. On the contrary, to obtain the same order of accuracy, an extremely large number of nodes is required if the integration is carried over the whole triangle $\mathcal{T}$. In the following section we perform several numerical test to show the efficiency of the new proposed procedure with respect to the integration on the whole triangle. In particular, in Example 1 we report a comparison

Figure 1: A benchmark example of strip $\mathcal{C}_j$

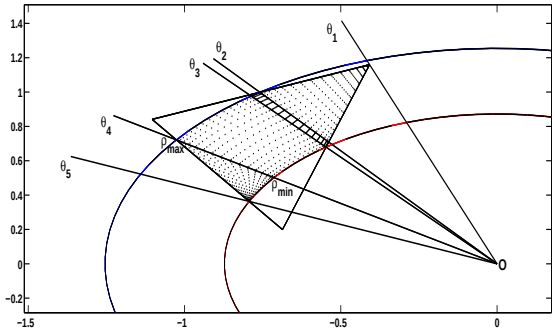

between $I_{\mathcal{CB}}$ and $I_{\mathcal{CB}_{loc}}$, where a fixed benchmark triangle is considered. In Examples 2–4 we test the proposed numerical approaches for the solution of the BIEs (4) and (5), for different choices of Γ and T.

4 Numerical tests

In the numerical tests of this section, we have used the compactly supported temporal basis functions $N_j(t) = \phi_j(\frac{t}{\Delta_t})$, where the functions ϕ_j are defined by

$$\begin{cases} \phi_0(t) = [\psi(t-1) + 1 - t]/2 \\ \phi_1(t) = [\psi(t-2) - 2\psi(t-1) + t]/2 \\ \phi_j(t) = [\psi(t-j-1) - 2\psi(t-j) + \psi(t-j+1)]/2, \quad j \geq 2, \end{cases} \tag{27}$$

with a proper ψ. These functions have been suggested in [5]. In particular, we have considered two kinds of basis functions: the standard piecewise linear temporal shape functions and some special C^∞ basis functions. The first ones are obtained from (27) by choosing

$$\psi(t) = |t|, \tag{28}$$

and have compact support of width $2\Delta_t$; we refer to this choice by using the label $\mathcal{CB}1$. The second type of basis functions is obtained from (27) by choosing

$$\psi(t) = \begin{cases} t\,\mathrm{erf}(2\tanh^{-1}(t)) + \frac{1}{2\sqrt{\pi}}\exp(-4[\tanh^{-1}(t)]^2) & \text{for } |t| < 1, \\ |t| & \text{for } |t| \geq 1, \end{cases} \tag{29}$$

and have a compact support of width $4\Delta_t$; we refer to this choice by using the label $\mathcal{CB}2$. The latter have been proposed in [5]. In Figures 2 and 3 we show the behavior of the functions N_j for both choices of the temporal basis functions described above (left plots), and some integrand functions involved in (19) for different choices of the time step Δ_t (middle and right plots).

Figure 2: The functions N_j for the choice $\mathcal{CB}1$ (left) and the integrand functions involved in (19) with $\mathcal{CB}1$ at the instant $t = 1/2$, for $\Delta_t = T/8$ (middle) and $\Delta_t = T/64$ (right), with $T = 1$.

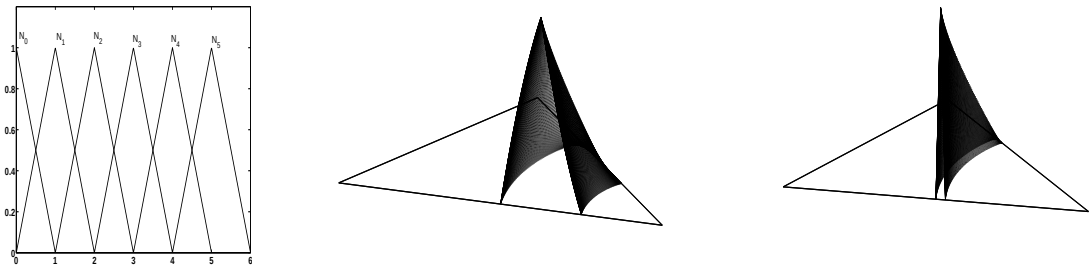

Figure 3: The functions N_j for the choice $\mathcal{CB}2$ (left) and the integrand functions involved in (19) with $\mathcal{CB}2$ at the instant $t = 1/2$, for $\Delta_t = T/8$ (middle) and $\Delta_t = T/64$ (right), with $T = 1$.

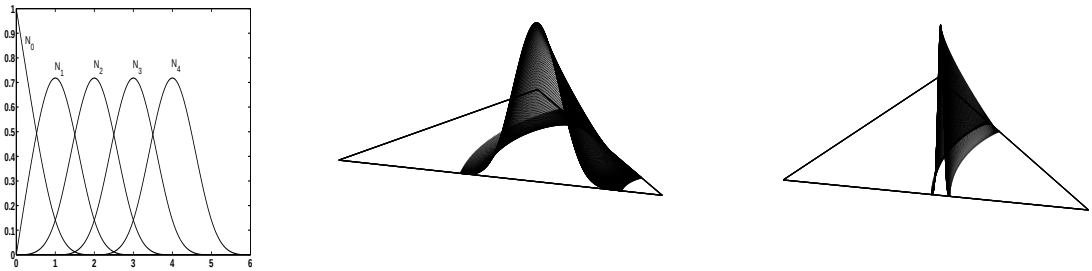

Remark 4.1 *The support $[t_{1,j}, t_{2,j}]$, that defines the strip of integration in $I_{\mathcal{CB}_{loc}}$ (see (24)), coincides with $[t_{j-1}, t_{j+1}]$ for the choice (28). In this case, according to the behavior of the corresponding temporal basis functions N_j, which is not smooth in t_j, we split the strip $\mathcal{C}_j$ as*

$$\mathcal{C}_j = \{(\bar{y}_1, \bar{y}_2) \in \bar{\mathcal{T}} : \varrho_{1,j}^2 \leq \mathcal{E}(\bar{y}_1, \bar{y}_2) \leq \varrho_{m,j}^2\} \cup \{(\bar{y}_1, \bar{y}_2) \in \bar{\mathcal{T}} : \varrho_{m,j}^2 \leq \mathcal{E}(\bar{y}_1, \bar{y}_2) \leq \varrho_{2,j}^2\}$$

where $\varrho_{m,j}^2 = t_j^2 - h$. For the choice (29), the support $[t_{1,j}, t_{2,j}]$ coincides with $[t_{j-2}, t_{j+2}]$. In this last case, even if N_j is smooth, we have observed a faster rate of convergence when the corresponding integrals are computed by splitting $\mathcal{C}_j$ into four sub-strips associated to the four subintervals in $[t_{j-2}, t_{j+2}]$.

Example 1 As a first test, in order to emphasize the importance of the detection of the support of the integrand function appearing in (19), namely to test the efficiency of the proposed quadrature approach, we compare the values of the integrals $I_{\mathcal{CB}}$ and $I_{\mathcal{CB}_{loc}}$ obtained by integrating on the whole triangle and on the localized support, respectively. We consider both $\mathcal{CB}1$ and $\mathcal{CB}2$, associated to a uniform partition of $[0, T]$ into N subintervals. We choose a triangle in a mesh of 32 triangles of the polyhedron Γ_Δ that approximates the unit sphere, and we fix a collocation point that belongs to the unit sphere as well; the final time is $T = 1$ and the number of time steps is $N = 64$. We remark again that the integrand function is non vanishing in the strip obtained by intersecting the triangle with the (non degenerate) ellipses defined in (23). For the above choice of the spatial mesh and of the temporal partition, the strip is thin with respect to the size of the triangle. In Figure 5, for example, we plot the support, the distribution of the quadrature nodes inside the support, and the behavior of the integrand functions in (19) involving N_1, N_{32} and N_{50} associated to the choice $\mathcal{CB}1$ and the instants t_j, $j = 1, 32, 50$ of the time mesh. In Table 1, we report the maximum, with respect to t_j, $j = 1, \cdots, 64$, of the relative errors associated to $I_{\mathcal{CB}}$ and $I_{\mathcal{CB}_{loc}}$, for increasing values of the number n of points of the basis Gauss-Legendre quadrature formula. The number n_e denotes the order of magnitude of the global number of quadrature points needed to compute all the integrals associated to the instants $j = 1, \ldots, 64$; it takes into account all the splits of the intervals of integration with respect to the variables θ and ϱ.

The corresponding reference values are obtained by computing (26) with $n = 2048$. When the double precision accuracy is achieved, we do not increase n further.

We point out that the accuracy obtained by performing the integration over the whole triangle is poor for small values of n, since only few quadrature nodes lie in the support of the integrand function because of its thinness. On the contrary, only few nodes inside the support are sufficient to obtain an accurate approximation; for example an accuracy of order $1e-06$ is achieved with $n = 4$ by $I_{\mathcal{CB}1_{loc}}$ and $n = 1024$ by $I_{\mathcal{CB}1}$. Moreover, with $n = 8$ we get the machine precision for the integral $I_{\mathcal{CB}1_{loc}}$, and $n = 32$ for the integral $I_{\mathcal{CB}2_{loc}}$. In Figure 4 we plot the relative errors for all the instants $t_j, j = 1, \cdots, 64$ for $\mathcal{CB}1$ and $\mathcal{CB}2$, and for some value of n.

Incidentally, we point out that we have also applied the quadrature strategy used in [5]. This strategy consists in introducing first the Duffy type transformation to eliminate the singular behavior of the integrand functions in those cases where the collocation point $\mathbf{x}_m$ coincides with a vertex of the triangular domain of integration; the resulting integrals are

Figure 4: Example 1. Relative errors of $I_{\mathcal{CB}1}$ and $I_{\mathcal{CB}1_{loc}}$ (left), $I_{\mathcal{CB}2}$ and $I_{\mathcal{CB}2_{loc}}$ (right), for $T = 1$ associated to the instants $t_j, j = 1, \cdots, 64$.

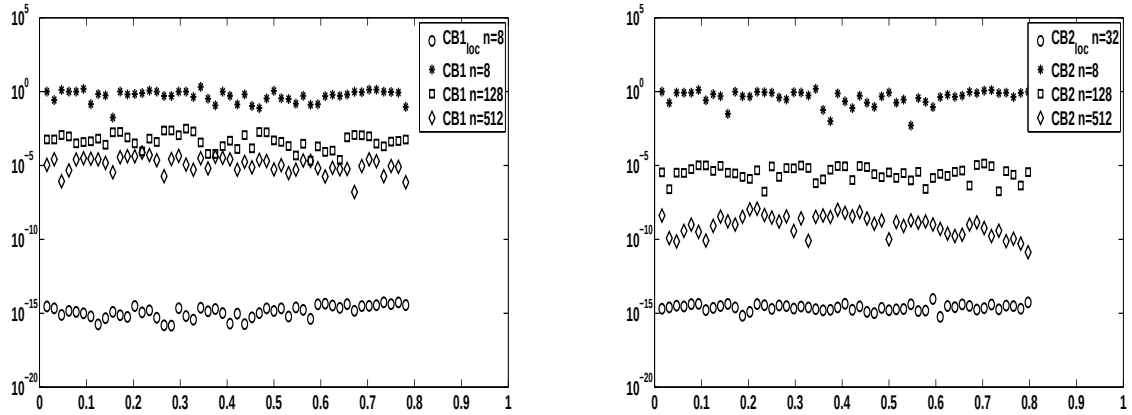

then approximated by a composite quadrature defined on 16 subtriangles, obtained by taking as the basic rule the fourth order-6 points Dunavant quadrature (see [6] for details). Such a technique has the same drawbacks of the integration over the whole triangle; therefore it has not been considered here as an alternative approach.

Table 1: Example 1. Maximum of the relative errors of $I_{\mathcal{CB}1}$, $I_{\mathcal{CB}1_{loc}}$, $I_{\mathcal{CB}2}$ and $I_{\mathcal{CB}2_{loc}}$, for $T = 1$ and $N = 64$.

n	n_e	$\mathcal{CB}1$	n_e	$\mathcal{CB}1_{loc}$	n_e	$\mathcal{CB}2$	n_e	$\mathcal{CB}2_{loc}$
2	$3.0e+01$	$1.47e+01$	$6.0e+02$	$1.80e-02$	$5.0e+01$	$1.33e+01$	$3.0e+02$	$8.66e-02$
4	$3.0e+02$	$8.19e+00$	$3.0e+03$	$1.08e-06$	$6.0e+02$	$5.75e+00$	$5.0e+03$	$4.35e-04$
8	$3.0e+03$	$2.13e+00$	$1.0e+04$	$5.55e-15$	$3.0e+03$	$1.55e+00$	$2.0e+04$	$4.15e-07$
16	$1.0e+04$	$7.66e-01$			$1.0e+04$	$5.06e-01$	$8.0e+04$	$1.49e-10$
32	$5.0e+04$	$1.15e-01$			$5.0e+04$	$7.58e-02$	$3.0e+05$	$1.35e-14$
64	$2.0e+05$	$1.86e-02$			$2.0e+05$	$8.85e-04$		
128	$8.0e+05$	$3.12e-03$			$8.0e+05$	$1.36e-05$		
256	$3.0e+06$	$4.36e-04$			$3.0e+06$	$1.28e-06$		
512	$1.0e+07$	$7.44e-05$			$1.0e+07$	$1.19e-08$		
1024	$5.0e+07$	$9.59e-06$			$5.0e+07$	$2.51e-10$		

Figure 5: Example 1. Support (left), distribution of the quadrature nodes (middle) and zoom of the behavior of the integrand functions (right), associated to the instants t_1, t_{32}, t_{50} on a benchmark triangle, for $T = 1$, $N = 64$.

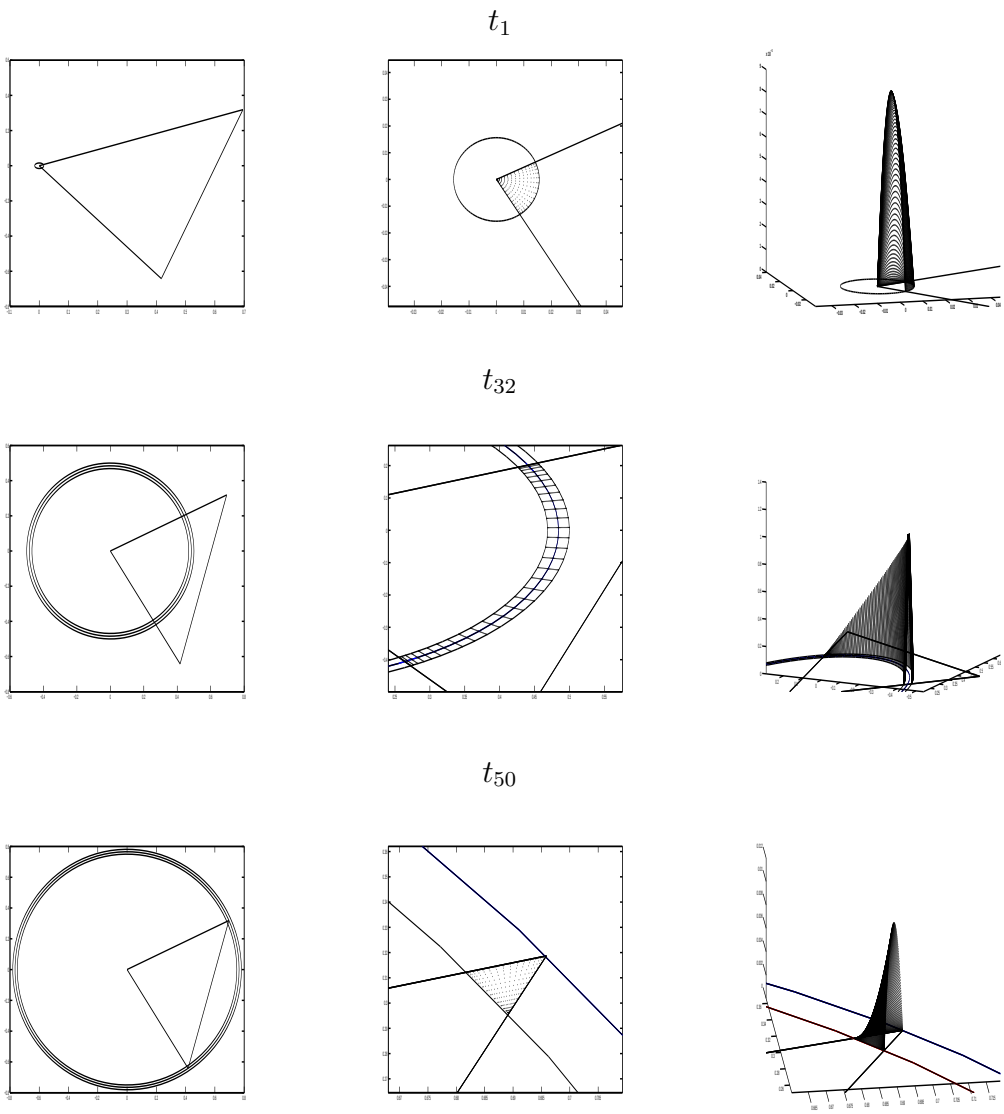

The next numerical tests are devoted to the resolution of the BIEs (4) and (5), for different choices of the domain Ω and of the time interval $[0, T]$. We will compare the numerical approaches that we have described in Sections 2.1 and 2.2, respectively; for the second approach we will consider both the piecewise linear temporal basis functions and the C^∞ basis functions. For the convenience of the reader, we recall the approaches we will apply:

- the Lubich technique $\mathcal{L}$, combined with the space integration over the whole triangle;
- the techniques using compactly supported temporal basis functions, combined with the space integration over the whole triangle: $\mathcal{CB}1$ when the piecewise linear functions (28) are used, and $\mathcal{CB}2$ when the C^∞ basis functions (29) are used;
- the techniques using compactly supported temporal basis functions, combined with the space integration proposed in Section 3, based on the exact detection of the support of the integrand functions; we refer to them by $\mathcal{CB}1_{loc}$ and $\mathcal{CB}2_{loc}$ according to the temporal basis functions involved.

Example 2. As second example, we solve equations (4) and (5) defined on the unit disc $\Gamma = \{(x, y, z) \in \mathbb{R}^3 : x^2 + y^2 \leq 1,\ z = 0\}$ where we prescribe the Dirichlet datum $g(\mathbf{x}, t) = t^3/(2\sqrt{\pi})$.

The goal of this test is to analyze the performances of the above mentioned numerical approaches when the space mesh of the disc and the final time T are fixed, and the number N of the time steps increases (or, equivalently, Δ_t decreases). In Tables 2 and 3 we report the approximate values of the density function φ in the center of the disc, for the fixed space mesh made up of 32 triangles and at the final times $T = 1$ and $T = 10$, respectively. We show that, if the matrix elements (defined by the space integrals) are evaluated with an accuracy ε, then there exists an $\Delta_{t,0} = \Delta_{t,0}(\varepsilon)$ (or, equivalently, a $N_0(\varepsilon)$) such that for all $\Delta_t < \Delta_{t,0}$ (or, equivalently, $N > N_0$) numerical instabilities appear. We remark that the value of $\Delta_{t,0}$ is different for each method. As the numerical results show, all the approaches seem to be stable, admitted that the computation of the space integrals is sufficiently accurate. Indeed, the numerical instabilities for large values of N disappear as soon as the space quadrature number n increases, that is the computation of space integrals is sufficiently accurate; precisely, the smaller is Δ_t, the higher is the accuracy required for the computation of the integrals. For simplicity, the number of quadrature nodes n is doubled whenever the approach looks unstable; probably, to obtain numerical stable results, the required number of quadrature nodes could be smaller than the last value considered. Since, for the chosen refinement, the number of the significant digits is 3 (2.03 for $T = 1$ in Table 2 and 527 for $T = 10$ in Table 3), we increase the number of quadrature nodes n until, for large values of N, we achieve the above three digits and a graph of $\varphi((0, 0, 0), t)$ for $t \in [0, T]$ without oscillations. By taking into account this objective, the symbols in the tables below have the following meaning: "$\times$" when the approximate value does not make sense because the corresponding quadrature node number is not sufficiently large; "*" when the approximate value is unacceptable and/or the behavior of the density function oscillates at the intermediate instants; empty when the target has been already reached. For example,

in Table 2, the value of the solution obtained applying the $\mathcal{CB}1$ procedure for $N = 256$ and $n = 64$ would seem acceptable but, as Figure 6 (left plot) shows, the graph of $\varphi((0,0,0),t)$ for $t \in [0,1]$ has unacceptable oscillations. On the contrary, the solution obtained applying $\mathcal{CB}1_{loc}$ with $n = 4$ does not show up oscillations (see Figure 6 right plot). We underline that, in order to obtain an accurate solution, all the approaches where the integration over the whole triangles is considered, require an increasing number of quadrature nodes as the value of N increases; on the contrary, for $\mathcal{CB}1_{loc}$ and $\mathcal{CB}2_{loc}$, where the localization of the support of the integrand function is considered, few quadrature nodes are sufficient.

Moreover, we point out that in the Lubich approach, the instabilities appear for values of N larger than those of $\mathcal{CB}1$ and $\mathcal{CB}2$. Finally, we remark that we have performed further tests taking finer spatial meshes, and we have observed a similar phenomenon.

Table 2: Example 2. Values of $\varphi((0,0,0),T)$, $T = 1$.

N	n	$\mathcal{L}$	$\mathcal{CB}1$	$\mathcal{CB}1_{loc}$	$\mathcal{CB}2$	$\mathcal{CB}2_{loc}$
8	4	2.0135	2.0610	2.0415	2.0430	2.0367
	8	2.0133	2.0435	2.0415	2.0368	
	16		2.0418			
16	4	2.0375	3.6065^*	2.0365	2.0309	2.0357
	8		2.0468			
	16		2.0362			
32	4	2.0414	$\times$	2.0350	$-1.0e+01^*$	2.0349
	8	2.0404	2.0187		2.0345	
	16		2.0367			
64	4	2.0363	$\times$	2.0347	$\times$	2.0346
	8		$-3.0e+02^*$		$-1.0e+04^*$	
	16		1.2892^*		2.0346	
	32		2.0343			
128	4	268.95^*	$\times$	2.0348	$\times$	2.0347
	8	2.0366	$\times$		$\times$	
	16		$\times$		$2.0e+08^*$	
	32		-2.6718^*		2.0348	
	64		2.0349			
256	4	$\times$	$\times$	2.0348	$\times$	2.0348
	8	$4.0e+05^*$	$\times$		$\times$	
	16	2.0357	$\times$		$\times$	
	32		$\times$		$8.0e+08^*$	
	64		2.0399^*		2.0348	
	128		2.0348			
512	4	$\times$	$\times$	2.0348	$\times$	2.0348
	8	$\times$	$\times$		$\times$	
	16	2.1235	$\times$		$\times$	
	32	2.0351	$\times$		$\times$	
	64		$\times$		$-4.0e+08^*$	
	128		$1.0e+01^*$		2.0348	
	256		2.0348			
1024	4	$\times$	$\times$	2.0348	$\times$	2.0348
	8	$\times$	$\times$		$\times$	
	16	$3.0e+42^*$	$\times$		$\times$	
	32	2.0349	$\times$		$\times$	
	64		$\times$		$\times$	
	128		$\times$		$1.0e+09^*$	
	256		$-1.0e+03^*$		2.0348	
	512		2.0469^*			
	1024		2.0348			

Figure 6: Example 2. Behavior of $\varphi(0,0,t)$ for $t \in [0,1]$ and $N = 256$, obtained by $\mathcal{CB}1$ with $n = 64$ (left plot) and by $\mathcal{CB}1_{loc}$ with $n = 4$ (right plot).

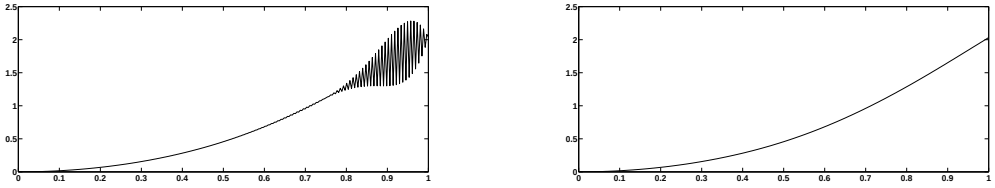

Table 3: Example 2. Values of $\varphi((0,0,0),T)$, $T = 10$

N	n	$\mathcal{L}$	$\mathcal{CB}1$	$\mathcal{CB}1_{loc}$	$\mathcal{CB}2$	$\mathcal{CB}2_{loc}$
8	4	524.76	518.73	520.07	519.75	521.12
	8	526.15	520.08	520.14	521.13	521.19
	16	526.20	520.14		521.19	
16	4	525.46	524.83	526.09	524.65	526.01
	8	526.85	526.08	526.16	526.03	526.08
	16	526.90	526.16		526.08	
32	4	525.64	526.20	528.05	525.45	526.86
	8	527.02	528.15	528.12	526.83	526.94
	16		528.07		526.89	
64	4	525.68	524.26	527.09	525.62	527.08
	8	527.06	527.27		527.00	
128	4	525.69	$-5.0e+10^*$	527.25	524.97	527.12
	8	527.07	523.42^*		527.15	
	16		526.67			
	32		527.43			
256	4	525.70	$\times$	527.25	$3.0e+59^*$	527.13
	8	527.08	$2.0e+16^*$		484.99^*	
	16		526.25		527.13	
	32		527.63			
512	4	525.70	$\times$	527.13	$\times$	527.14
	8	527.08	$\times$		$\times$	
	16		$-2.0e+24^*$		550.96^*	
	32		502.30^*		527.14	
	64		523.77^*			
	128		524.03^*			
	256		527.16			
1024	4	$2.0e+46^*$	$\times$	527.14	$\times$	527.14
	8	527.08	$\times$		$\times$	
	16		$\times$		$\times$	
	32		$\times$		530.02^*	
	64		$\times$		527.14	
	128		$\times$			
	256		527.14			
2048	4	$\times$	$\times$	527.14	$\times$	527.14
	8	$-1.0e+37$	$\times$		$\times$	
	16	527.14	$\times$		$\times$	
	32		$\times$		$7.0e+63^*$	
	64		$\times$		528.42^*	
	128		$\times$		527.14	
	256		$-2.0e+04^*$			
	512		527.16			

As already remarked at the end of Section 2.2, all the block matrices generated by the approaches that use compactly supported temporal basis functions are sparse, as well as the final lower triangular Toeplitz system. To give an idea of the sparsity, recalling that M is the number of the vertices of the triangulation, we introduce the quantity

$$\mathcal{S}_{N,M} = \frac{\sum_{j=0}^{N} nz(\bar{\mathbf{A}}_j)}{(N+1)M^2},$$

where $nz(\bar{\mathbf{A}}_j)$ denotes the number of nonzero entries of the matrix $\bar{\mathbf{A}}_j$, while $(N+1)M^2$ is the total number of the matrix elements which have to be computed to construct the final linear system. Incidentally, the latter is the number of matrix elements that must be computed by the Lubich approach if, as in our case, no particular approximation strategy is adopted. In Tables 4 and 5 we report the percentages of $\mathcal{S}_{N,M}$ for the approaches $\mathcal{CB}1_{loc}$ and $\mathcal{CB}2_{loc}$ by using 32 ($M = 25$) and 128 ($M = 81$) triangles respectively, and for the final times $T = 1$ and $T = 10$ and different values of N.

Table 4: Example 2. The percentage of $\mathcal{S}_{N,M}$ for 32 triangles and $T = 1, 10$.

	$T=1$		$T=10$	
N	$\mathcal{CB}1_{loc}$	$\mathcal{CB}2_{loc}$	$\mathcal{CB}1_{loc}$	$\mathcal{CB}2_{loc}$
32	38%	41%	13%	19%
64	37%	38%	10%	13%
128	37%	38%	9%	10%
256	37%	37%	8%	9%

Table 5: Example 2. The percentage of $\mathcal{S}_{N,M}$ for 128 triangles and $T = 1, 10$.

	$T=1$		$T=10$	
N	$\mathcal{CB}1_{loc}$	$\mathcal{CB}2_{loc}$	$\mathcal{CB}1_{loc}$	$\mathcal{CB}2_{loc}$
32	25%	28%	10%	20%
64	23%	25%	7%	10%
128	23%	24%	6%	7%
256	22%	23%	5%	6%

Example 3. We test here the approaches $\mathcal{L}$, $\mathcal{CB}1$, $\mathcal{CB}1_{loc}$, $\mathcal{CB}2$ and $\mathcal{CB}2_{loc}$, when $\Gamma = \{(x,y,z) \in \mathbb{R}^3 : x^2+y^2+z^2 = 1\}$ and the Dirichlet datum $g(\mathbf{x},t) = \frac{t^3}{\sqrt{2\pi}}$. The space domain is approximated by the surface of a regular (inscribed) polyhedron having triangular faces, obtained by using the algorithm contained in the software library BEMLIB, which can be downloaded from the internet site: http://bemlib.ucsd.edu (see [13]). In particular, for the refinement labeled level 1 we have 32 triangles and 18 vertices, at level 2: 128 triangles and 66 vertices, at level 3: 512 triangles and 258 vertices, and at level 4: 2048 triangles and 1026 vertices. In this case, the exact solution of (4) and (5) is known and is given by $\varphi(\mathbf{x},t) = \sum_{k=0}^{\lfloor t/2 \rfloor} g'(t-2k)$ (see (4.11) in [14]). As in Example 2, since the aim of this test is to analyze the influence that the accurate computation of the matrix elements of the final linear system has on the approximate solution, and not to study the convergence of the methods, we fix the spatial mesh and, for fixed T, we increase the number N of the temporal instants. In Tables 6 and 7 we report the relative errors

$$\mathrm{E_{P,T}} := \frac{|\varphi(P,T) - \varphi_{M,N}(P,T)|}{|\varphi(P,T)|}, \tag{30}$$

where $P = (1,0,0)$, and

$$\mathrm{E_{max}} := \frac{\max\limits_{j=1,\cdots,N} \max\limits_{i=1,\cdots,M} |\varphi(V_i,t_j) - \varphi_{M,N}(V_i,t_j)|}{\max\limits_{j=1,\cdots,N} \max\limits_{i=1,\cdots,M} |\varphi(V_i,t_j)|}, \tag{31}$$

being V_i the vertices of the triangulation of the sphere, for all the numerical procedures we have considered and for $T = 1$ and $T = 10$. The triangulation of the sphere consists of only 32 triangles (level 1). We refer the reader to Example 2 for the notations in the tables. As already remarked in Example 2, the localization of the support of the integrand functions is a key issue to obtain an accurate solution with a few quadrature nodes, thus avoiding numerical instabilities for large values of N. It is worthwhile noting that, when $T = 1$ the methods $\mathcal{CB}1_{loc}$ and $\mathcal{CB}2_{loc}$, in which the new quadrature strategy is applied, are the only ones where the instabilities do not show up till $\Delta_t = 1/4096 \approx 2.4 - 04$. On the contrary, when $T = 10$, 8 quadrature nodes are sufficient only for $\mathcal{CB}2_{loc}$. We remark that this result depends on the fact that, for these choices of the parameters, the temporal basis functions associated to $\mathcal{CB}1_{loc}$ have a more sharply-peaked behavior than that associated to $\mathcal{CB}2_{loc}$ and they are defined on a smaller support. We point out that the accuracy is poor and the associated error does not decrease by increasing N because the space mesh is very coarse and fixed. Indeed, by refining both in space and time, the accuracy of the approximate solution improves and, consequently, the corresponding error decreases.

Table 6: Example 3. Relative errors (30) and (31), for $P = (1, 0, 0)$ and $T = 1$.

		$\mathcal{L}$		$\mathcal{CB}1$		$\mathcal{CB}1_{loc}$		$\mathcal{CB}2$		$\mathcal{CB}2_{loc}$	
N	n	$E_{P,T}$	E_{max}	$E_{P,T}$	E_{max}	$E_{P,T}$	E_{max}	$E_{P,T}$	E_{max}	$E_{P,T}$	E_{max}
8	4	$5.12e-02$	$1.29e-01$	$3.61e-03^*$	$2.12e-01^*$	$6.16e-02$	$1.43e-01$	$5.09e-02$	$1.45e-01$	$5.71e-02$	$1.38e-01$
	8			$6.07e-02$	$1.43e-01$						
16	4	$5.74e-02$	$1.40e-01$	$\times$	$\times$	$6.10e-02$	$1.44e-01$	$5.61e-02$	$1.43e-01$	$6.01e-02$	$1.42e-01$
	8			$7.79e-02$	$1.52e-01$						
32	4	$5.79e-02$	$1.43e-01$	$\times$	$\times$	$6.11e-02$	$1.44e-01$	$1.0e+02^*$	$2.0e+02^*$	$6.08e-02$	$1.44e-01$
	8			$2.78e-01^*$	$3.10e-01^*$			$5.98e-02$	$1.44e-01$		
	16			$7.30e-02^*$	$1.50e-01^*$						
	32			$6.07e-02$	$1.44e-01$						
64	4	$1.01e-01^*$	$2.20e-01^*$	$\times$	$\times$	$6.10e-02$	$1.44e-01$	$\times$	$\times$	$6.09e-02$	$1.44e-01$
	8	$6.10e-02$	$1.39e-01$	$\times$	$\times$			$4.29e+08^*$	$4.29e+08^*$		
	16			$\times$	$\times$			$1.17e-01^*$	$2.62e-01^*$		
	32			$1.00e-01^*$	$1.72e-01^*$			$6.09e-02$	$1.44e-01$		
	64			$6.11e-02$	$1.44e-01$						
128	4	$\times$	$\times$	$\times$	$\times$	$6.10e-02$	$1.44e-01$	$\times$	$\times$	$6.10e-02$	$1.44e-01$
	8	$6.02e-02$	$1.38e-01$	$\times$	$\times$			$\times$	$\times$		
	16			$\times$	$\times$			$\times$	$\times$		
	32			$\times$	$\times$			$6.32e-02$	$1.44e-01$		
	64			$6.10e-02$	$1.44e-01$						
256	4	$\times$	$\times$	$\times$	$\times$	$6.10e-02$	$1.44e-01$	$\times$	$\times$	$6.10e-02$	$1.44e-01$
	8	$9.92e+07^*$	$1.70e+08^*$	$\times$	$\times$			$\times$	$\times$		
	16	$6.10e-02$	$1.44e-01$	$\times$	$\times$			$\times$	$\times$		
	32			$\times$	$\times$			$9.74e+06^*$	$7.69e+07^*$		
	64			$1.03e+04^*$	$1.03e+04^*$			$6.05e-02$	$1.44e-01$		
	128			$7.43e-02$	$1.49e-01$						
512	4	$\times$	$\times$	$\times$	$\times$	$6.10e-02$	$1.44e-01$	$\times$	$\times$	$6.10e-02$	$1.44e-01$
	8	$\times$	$\times$	$\times$	$\times$			$\times$	$\times$		
	16	$2.47e+06^*$	$8.99e+08^*$	$\times$	$\times$						
	32	$6.10e-02$	$1.44e-01$	$\times$	$\times$						
	64			$\times$	$\times$			$5.81e+08^*$	$1.03e+10^*$		
	128			20.28^*	28.15^*			$6.06-02^*$	$1.46-01^*$		
	256			$4.24e-02^*$	$1.51e-01^*$			$6.10-02$	$1.44e-01$		
	512			$6.10e-02$	$1.44e-01$						
1024	4	$\times$	$\times$	$\times$	$\times$	$6.10e-02$	$1.44e-01$	$\times$	$\times$	$5.95e-02$	$1.43e-01$
2048	4	$\times$	$\times$	$\times$	$\times$	$6.10e-02$	$1.44e-01$	$\times$	$\times$	$6.10e-02$	$1.44e-01$
4096	4	$\times$	$\times$	$\times$	$\times$	$6.10e-02$	$1.44e-01$	$\times$	$\times$	$6.10e-02$	$1.44e-01$

Table 7: Example 3. Relative errors (30) and (31), for $P = (1, 0, 0)$, $n = 8$ and $T = 10$.

	$\mathcal{L}$		$\mathcal{CB}1$		$\mathcal{CB}1_{loc}$		$\mathcal{CB}2$		$\mathcal{CB}2_{loc}$	
N	$E_{P,T}$	E_{max}	$E_{P,T}$	E_{max}	$E_{P,T}$	E_{max}	$E_{P,T}$	E_{max}	$E_{P,T}$	E_{max}
8	$7.38e-02$	$1.56e-01$	$9.74e-02$	$1.83e-01$	$9.77e-02$	$1.83e-01$	$6.71e-02$	$1.49e-01$	$6.74e-02$	$1.48e-01$
16	$7.57e-02$	$1.58e-01$	$7.42e-02$	$1.56e-01$	$7.45e-02$	$1.56e-01$	$7.33e-02$	$1.55e-01$	$7.36e-02$	$1.55e-01$
32	$7.61e-02$	$1.58e-01$	$7.74e-02$	$1.59e-01$	$7.80e-02$	$1.59e-01$	$7.51e-02$	$1.57e-01$	$7.54e-02$	$1.57e-01$
64	$7.63e-02$	$1.58e-01$	$2.75e-01^*$	$4.04e-01^*$	$3.14e-01^*$	$5.11e-01^*$	$7.58e-02$	$1.58e-01$	$7.60e-02$	$1.58e-01$
128	$7.59e-02$	$1.57e-01$	$\times$	$\times$	$\times$	$\times$	$7.58e-02$	$1.58e-01$	$7.62e-02$	$1.58e-01$
256	$7.59e-02$	$1.57e-01$	$\times$	$\times$	$\times$	$\times$	$8.12e+04^*$	$2.34e+05^*$	$7.63e-02$	$1.58e-01$
512	$7.59e-02$	$1.58e-01$	$\times$	$\times$	$\times$	$\times$	$\times$	$\times$	$7.63e-02$	$1.58e-01$
1024	$7.65e-02$	$1.57e-01$	$\times$	$\times$	$\times$	$\times$	$\times$	$\times$	$7.63e-02$	$1.58e-01$
2048	$3.00e+92^*$	$5.32e+94^*$	$\times$	$\times$	$\times$	$\times$	$\times$	$\times$	$7.63e-02$	$1.58e-01$

Figure 7: Example 4. Comparison between the exact solution and the approximations given by $\mathcal{L}$ (left), $\mathcal{CB}1$ and $\mathcal{CB}1_{loc}$ (middle), $\mathcal{CB}2$ and $\mathcal{CB}2_{loc}$ (right) for $T = 1,\ N = 64$.

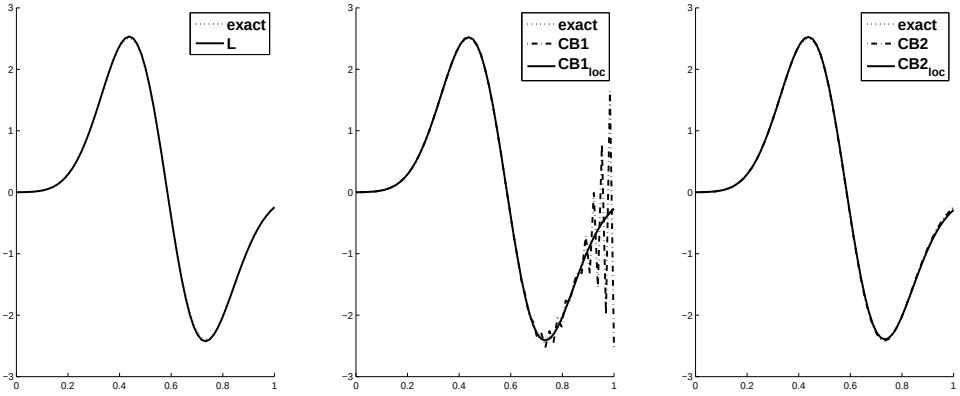

Example 4. We consider here the example presented in [5], where $\Gamma = \{(x, y, z) \in \mathbb{R}^3 : x^2 + y^2 + z^2 = 1\}$ and the Dirichlet datum on Γ is $g(\mathbf{x}, t) = t^2 \exp(-20(t - 1/2)^2)$. In the following numerical tests, we fix the space discretization (level 3), the time mesh size $\Delta_t = 1/64$ and the number of quadrature nodes $n = 8$, while we increase the number of time steps N (consequently T). This test is performed to show that, if the matrix elements (defined by the space integrals) are evaluated with an accuracy ε, then there exists an $N_0 = N_0(\varepsilon)$ (or, equivalently, a $T_0 = N_0\Delta_t$) such that for all $N > N_0$ (or, equivalently, $t > T_0$) instability oscillations appear. We point out that the value of N_0 is different for each method. For simplicity, we double the number of steps N until oscillations in the numerical solution show up, to see which of the five methods allows to consider the longest final time T without numerical instabilities.

In Figures 7–11 we compare the exact solution and its approximations obtained by the different numerical approaches. In Figure 7, where $T = 1$ and $N = 64$, all the methods are stable except the $\mathcal{CB}1$ approach for which oscillations appear for $t > 0.7$, approximately. In this case our quadrature technique $\mathcal{CB}1_{loc}$ produces an accurate solution without oscillations; indeed, it allows to integrate up to $T = 4$ (see Figure 8, middle plot), while it fails at $T = 8$ (see Figure 9, middle plot). On the contrary, the approximation obtained by $\mathcal{CB}2$ oscillates starting from $t \approx 3$ (see Figure 8, right plot), while $\mathcal{CB}2_{loc}$ performs well even at $T = 8$ (see Figure 9, right plot). Actually, with the chosen space and time refinement, $\mathcal{CB}2_{loc}$ allows the integration up to $T = 32$, while it fails at $T = 64$ with $N = 4096$, and the graph of the approximate solution shows up oscillations (see Figure 10). As regards the approach $\mathcal{L}$, oscillations do not show up until $T = 64$ (see Figure 10 (left)), but the accuracy of the approximation is really poor and a dumping effect is clearly visible; the latter is due to the particular choice of the datum g (as we will see in the forthcoming Example 5).

Incidentally, we point out that the accuracy of the approximations by $\mathcal{L}$ and $\mathcal{CB}2_{loc}$ improves with a finer space/time discretization. Indeed, in Figure 11, where we have chosen the space mesh of level 4, the approximate and exact solutions overlap.

Figure 8: Example 4. Comparison between the exact solution and the approximations given by $\mathcal{L}$ (left), $\mathcal{CB}1_{loc}$ (middle), $\mathcal{CB}2$ and $\mathcal{CB}2_{loc}$ (right) for $T = 4,\ N = 256$.

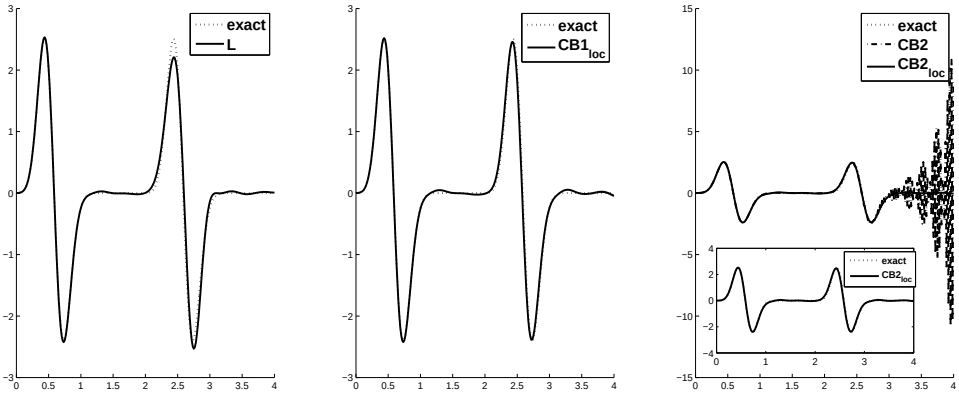

Figure 9: Example 4. Comparison between the exact solution and the approximations given by $\mathcal{L}$ (left), $\mathcal{CB}1_{loc}$ (middle) and $\mathcal{CB}2_{loc}$ (right) for $T = 8,\ N = 512$.

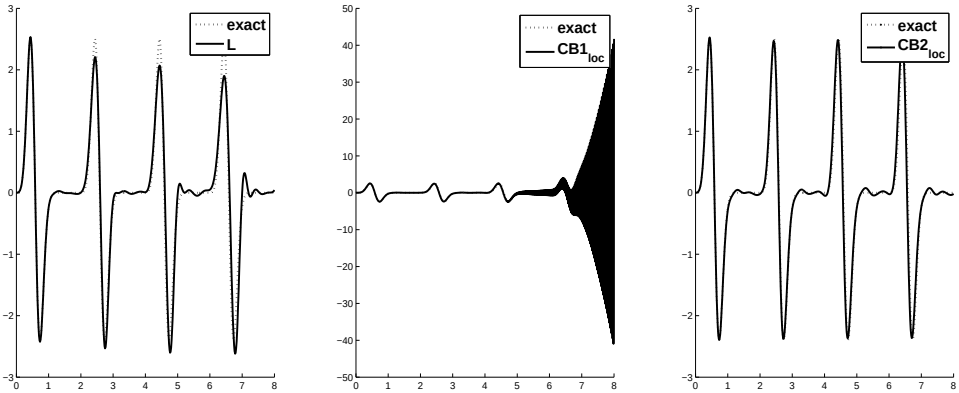

Figure 10: Example 4. Comparison between the exact solution and the approximation given by $\mathcal{L}$ (left) and $\mathcal{CB}2_{loc}$ (right) for $T = 64,\ N = 4096$.

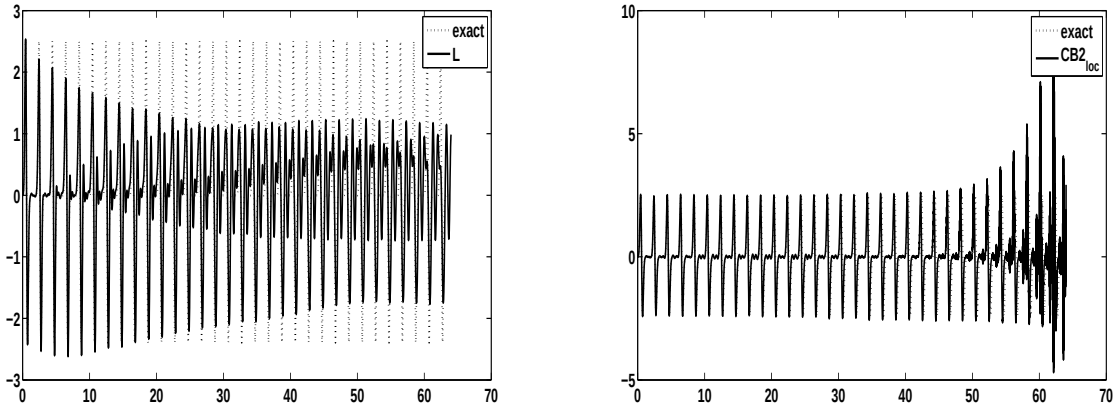

Figure 11: Example 4. Comparison between the exact solution and the approximations for $T = 8$ and level 4, given by $\mathcal{L}$ with $N = 2048$ (left) and $\mathcal{CB}2_{loc}$ with $N = 512$ (right).

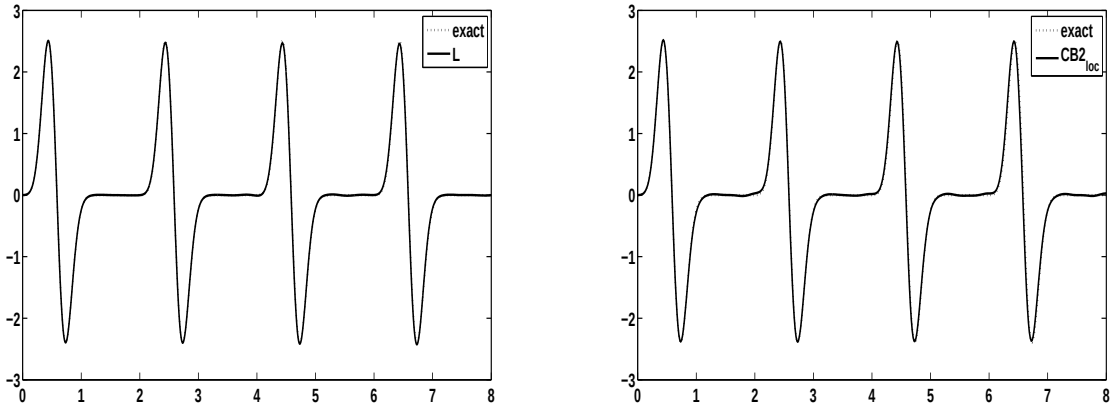

Example 5. In this last example, $\Gamma = \{(x, y, z) \in \mathbb{R}^3 : x^2 + y^2 + z^2 = 1\}$ and the Dirichlet datum on Γ is $g(\mathbf{x}, t) = t^4 \exp(-2t)$. This test is performed to show that the poor accuracy of the Lubich approach in Example 4 is due to the particular choice of the datum g, which requires a much finer time and space discretization. Indeed, for the same choices of the space and time parameters of Figure 10, the approach $\mathcal{L}$ performs better than all the others. In particular, in Figure 12 we show a comparison between $\mathcal{L}$ and $\mathcal{CB}2_{loc}$. We point out that at $T = 64$ and $N = 4096$, the oscillations produced by the method $\mathcal{CB}2_{loc}$ are even bigger than those of Figure 10; moreover, they do not disappear even for increasing values of the quadrature nodes in the computation of the matrix elements, and this is independent of the datum g. Therefore, as regards the method $\mathcal{CB}2_{loc}$ we can conclude that, to avoid numerical instabilities, when Δ_x is fixed it is necessary to choose a time step Δ_t sufficiently small. Incidentally, we point out that the same considerations hold for the method $\mathcal{CB}1_{loc}$ as well.

Figure 12: Example 5. Comparison between the exact solution and the approximation given by $\mathcal{L}$ (left) and $\mathcal{CB}2_{loc}$ (right) for $T = 64$, $N = 4096$ and $n = 8$.

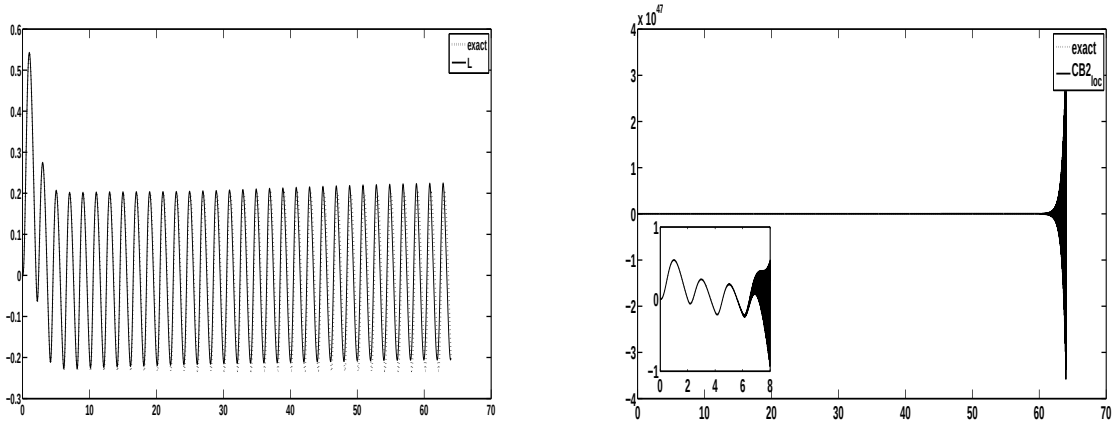

5 Conclusions

We have considered the retarded potential equation (5) and its numerical solution by means of compactly supported temporal basis functions (piecewise linear basis functions ($\mathcal{CB}1$) and C^∞ basis functions ($\mathcal{CB}2$)) combined with a collocation method in space. The accurate computation of the matrix system elements, involved in the final linear system and defined by space integrals, is crucial for the success of the numerical procedure (combined either with a collocation or a Galerkin method in space), otherwise oscillations in the solution density function soon show up. Since standard quadrature rules require a very large number of quadrature nodes to achieve the required precision, especially for small Δ_t (or, equivalently, large N), we have proposed a new integration strategy. Such a strategy is based on the exact detection of the local support of the integrand functions appearing in the integrals and turns out to be very efficient.

Moreover, we have compared this approach with the Lubich collocation method ($\mathcal{L}$), applied to the TDBIE (4). From the intensive numerical testing we have performed (many other tests have been done beyond the ones presented in this paper), we can summarize the following pros and cons for each of the analyzed methods.

1. The accurate approximation of the matrix elements is a key issue for the all the approaches. While in $\mathcal{L}$ a standard quadrature formula needs a relatively small number of nodes to get the required accuracy for the system elements, in $\mathcal{CB}1$ and $\mathcal{CB}2$ it needs a significantly large number of nodes. On the contrary, our integration strategy allows to obtain an accurate approximation by using a significantly smaller number of nodes.

2. For all the approaches, the final linear system has a Toeplitz lower triangular block structure. In $\mathcal{L}$ the lower triangular matrix is full and all the blocks are dense. However, the FFT routine allows to take advantage of the simultaneous computation of all the blocks. In $\mathcal{CB}1$ and $\mathcal{CB}2$ the lower triangular matrix has a band structure for large times $T > D = diam(\Gamma)$ and the blocks are sparse. Since the sparsity pattern is known a priori, many entries are not computed, thus saving computational cost and memory storage.

3. In the resolution of the BIEs, for all the analyzed methods, the smaller is the time step Δ_t, the higher is the accuracy required in the computation of the matrix elements in order to avoid numerical instabilities. Under the condition that all the matrix elements are computed with a sufficiently high accuracy, we highlight that:

   (a) $\mathcal{CB}2_{loc}$ performs better than $\mathcal{CB}1_{loc}$; this is probably due to the choice of the corresponding temporal basis functions, which are defined on a bigger support (twice the support of the piecewise linear temporal basis function), where they are smooth.

   (b) The approach $\mathcal{CB}1_{loc}$ is suitable only when the final time T is small, while for longer times it exhibits numerical instabilities unless the time step Δ_t is chosen sufficiently small. These properties hold both for open and closed surfaces Γ.

(c) The approach $\mathcal{CB}2_{loc}$ is suitable both for small and long T on open surfaces; indeed, in the numerical tests performed on the unit disk, we have considered long times up to $T = 10000$ with only $n = 8$ quadrature nodes without noting any instability phenomena. On the contrary, the method shows up numerical instabilities on closed surfaces for long times T, unless the time step Δ_t is chosen sufficiently small.

(d) The approach $\mathcal{L}$ seems to be stable both for open and closed surfaces, short and long times T (up to $T = 10000$), for arbitrary choices of the time step Δ_t. According to our intensive numerical testing, when a space collocation discretization is used, we believe that the approach $\mathcal{L}$ is the most reliable.

Acknowledgements

The authors gratefully acknowledge Professor G. Monegato for his precious advices and fruitful discussions. Moreover, the authors wish to thank Professor A. J. Di Scala for his helpful suggestions concerning the geometric aspects of the problem.

References

[1] A. Aimi, M. Diligenti, A. Frangi, and C. Guardasoni. Neumann exterior wave propagation problems: computational aspects of the 3D energetic Galerkin BEM. *J. Comput. Appl. Math.*, 235(7):1746–1754, 2011.

[2] A. Aimi, M. Diligenti, A. Frangi, and C. Guardasoni. A stable 3D energetic Galerkin BEM approach for wave propagation interior problems. *Engineering Analysis with Boundary Elements*, 36:1756–1765, 2012.

[3] A. Aimi, M. Diligenti, C. Guardasoni, I. Mazzieri, and S. Panizzi. An energy approach to space-time Galerkin BEM for wave propagation problems. *Internat. J. Numer. Methods Engrg.*, 80:1196–1240, 2009.

[4] A. Bamberger and T. Ha Duong. Formulation variationelle pour le calcul de la diffraction d'une onde acoustique par une surface rigide. *Math. Meth. in the Appl. Sci.*, 8:598–608, 1986.

[5] P. J. Davies and D. B. Duncan. Convolution-in-time approximations of time domain boundary integral equations. *SIAM J. Sci. Comput*, 35(1):B43–B61, 2013.

[6] D. A. Dunavant. High degree efficient symmetrical Gaussian quadrature rules for the triangle. *Internat. J. Numer. Methods Engrg.*, 21(6):11291148, 1985.

[7] S. Falletta, G. Monegato, and L. Scuderi. Space-time boundary integral equation methods for non homogeneous wave equation problems. The Dirichlet case. *IMA J. Numer. Anal.*, 32(1):202–226, 2012.

[8] S. Falletta, G. Monegato, and L. Scuderi. A space-time BIE method for wave equation problems: the (two-dimensional) Neumann case. *IMA J. Numer. Anal.*, 34(1):390–434, 2014.

[9] W. Hackbusch, W. Kress, and S. Sauter. Sparse convolution quadrature for time domain boundary integral formulations of the wave equation. *IMA J. Numer. Anal.*, 29:158–179, 2009.

[10] Ch. Lubich. Convolution quadrature and discretized operational calculus. I. *Numer. Math.*, 52:129–145, 1988.

[11] Ch. Lubich. On the multistep time discretization of linear initial-boundary value problems and their boundary integral equations. *Numer. Math.*, 67(3):365–389, 1994.

[12] G. Monegato, L. Scuderi, and M.P. Stanić. Lubich convolution quadratures and their application to space-time BIEs. *Numerical Algorithms*, 56(3):405–436, 2011.

[13] C. Pozrikidis. *A Practical Guide to Boundary Element Methods with the Software Library BEMLIB*. Chapman & Hall/CRC, Boca Raton, 2002.

[14] S. Sauter and A. Veit. A Galerkin method for retarded boundary integral equations with smooth and compactly supported temporal basis functions. *Numer. Math.*, 123(1):145–176, 2013.

[15] M. Schanz and H. Antes. Application of 'operational quadrature methods' in time domain boundary element methods. *Meccanica*, 32:179–186, 1997.